Contributions to Mineralogy and Petrology (2019) 174:99
https://doi.org/10.1007/s00410-019-1635-x

ORIGINAL PAPER

The influence of the thick banded series anorthosites on the crystallization of the surrounding rock of the Stillwater Complex, Montana

Samantha R. Baker[1,2] · **Alan E. Boudreau**[3]

Received: 20 May 2019 / Accepted: 16 October 2019 / Published online: 11 November 2019

Abstract

The Banded Series of the Archean-aged Stillwater Complex contains three thick anorthosites overlain by olivine-bearing rocks with apparently different crystallization sequence in that orthopyroxene appears late, if at all, as compared with that of the Ultramafic and Lower Banded series where orthopyroxene appears before plagioclase. Conventional models suggest that the rocks above the anorthosites represent injection of a magma with a different liquid line of descent than the rest of the complex. Alternatively, it has been suggested that the plagioclase + pyroxene mush protolith above the anorthosites was hydrated by the degassing of the underlying thick anorthosite units to produce olivine rather than pyroxene by either expansion of the olivine phase field by addition of H_2O, incongruent melting of pyroxene, and/or silica loss to the vapor. To test for hydration melting and a late silica loss, electron microprobe core/rim analyses were done on plagioclase grains from troctolite of Olivine-bearing zone V (OB-V). Approximately a dozen grains were analyzed for each of six thin sections. In total, 69 pairs were reversely zoned, and 22 were normal or unzoned. The most negative An difference was −8.25, the most positive was 4.32, but the majority of pairs were clustered from −5 to 1. The average was −2.1. Core grains had an average An number of 77.8, typical for other plagioclase from the Middle Banded series. A green, Na-rich hornblende is commonly associated with plagioclase where the latter is enclosed in olivine. The prevalence of reversely zoned grains is consistent with silica and sodium loss from pre-existing plagioclase. This evidence, as well as the lack of plagioclase core compositions being reset to more primitive, An-rich compositions, the amoeboidal, poikilitic habit of the olivine, and the presence of amphibole are all consistent with the troctolite and olivine gabbro of the Middle Banded series and lower parts of the Upper Banded series having formed as the result of a combination of processes including hydration, incongruent melting, and element leaching during degassing of the underlying anorthosites.

Keywords Stillwater Complex · Layered intrusions · Troctolite · Igneous fluid · Secondary olivine

Introduction

The reappearance of minerals such as olivine and chromite in the stratigraphic sequence of layered intrusions is commonly cited as evidence for the addition of more primitive magma during the crystallization of these intrusions. However, these minerals can also form during hydration melting

Communicated by Chris Ballhaus.

Electronic supplementary material The online version of this article (https://doi.org/10.1007/s00410-019-1635-x) contains supplementary material, which is available to authorized users.

✉ Alan E. Boudreau
boudreau@duke.edu

Samantha R. Baker
srbaker@uchicago.edu

[1] Durham Academy Upper School, 3601 Ridge Rd., Durham, NC 27705, USA

[2] Present Address: Department of Geophysical Sciences, University of Chicago, 5734 S. Ellis St., Chicago, IL 60637, USA

[3] Division of Earth and Ocean Sciences, Nicholas School of the Environment, Duke University, Durham, NC 27708, USA

or by a metasomatic leaching by silica-undersaturated volatile fluids of a pyroxene-bearing protolith (e.g., Boudreau 1988, 1999; Nicholson and Mathez 1991; Meurer et al. 1997). The former may require magmas with different crystallization behavior from the original magma, whereas the latter would suggest that changes in the apparent crystallization behavior can occur by fluid–magma–mush (hydromagmatic) interactions during the prolonged solidification of a single parent magma.

The Stillwater Complex in Montana is typical of layered intrusions in which olivine sporadically reappears in the stratigraphic sequence. Some of the more pronounced of these include the troctolite (olivine + plagioclase) units that occur above thick (to ~ 600 m) anorthosites of the Banded series. Boudreau (2016) noted the lack of compositional offsets to more primitive compositions as well as textural and mineral compositional similarities with stratigraphically nearby discordant troctolites. He suggested that extensive degassing of the (evolved) interstitial liquid from the underlying, uncompacted anorthosite created a vapor front that moved through norite and gabbronorite protoliths, leading to the flux melting and metasomatism to produce troctolite and olivine gabbro. This study analyzed the plagioclase zoning of samples from the troctolite units of Olivine-bearing zone V (OB-V) overlying the thickest anorthosite unit of the Middle Banded series to test for evidence of silica leaching by late stage igneous fluids.

General geology and previous interpretations

The Stillwater Complex is a 2.7 Ga (DePaolo and Wasserburg 1979) layered intrusion situated in south-central Montana (Fig. 1). More recent zircon geochronology has suggested the complex was assembled piecemeal over ~ 3 million years (Wall et al. 2018), although this has proved controversial and it has been suggested that there is no intrinsic reason whatsoever for the random emplacement of separate multiple sills into pre-existing solidified rocks to mimic the regular crystallization sequences of the Stillwater Complex. (Latypov 2019).

The complex has been divided into three main stratigraphic divisions: from the bottom up they are: the Basal Series, the Ultramafic Series and the Banded Series. Each series has been further divided into a number of informal zones and subzones, those used here are shown in Fig. 2.

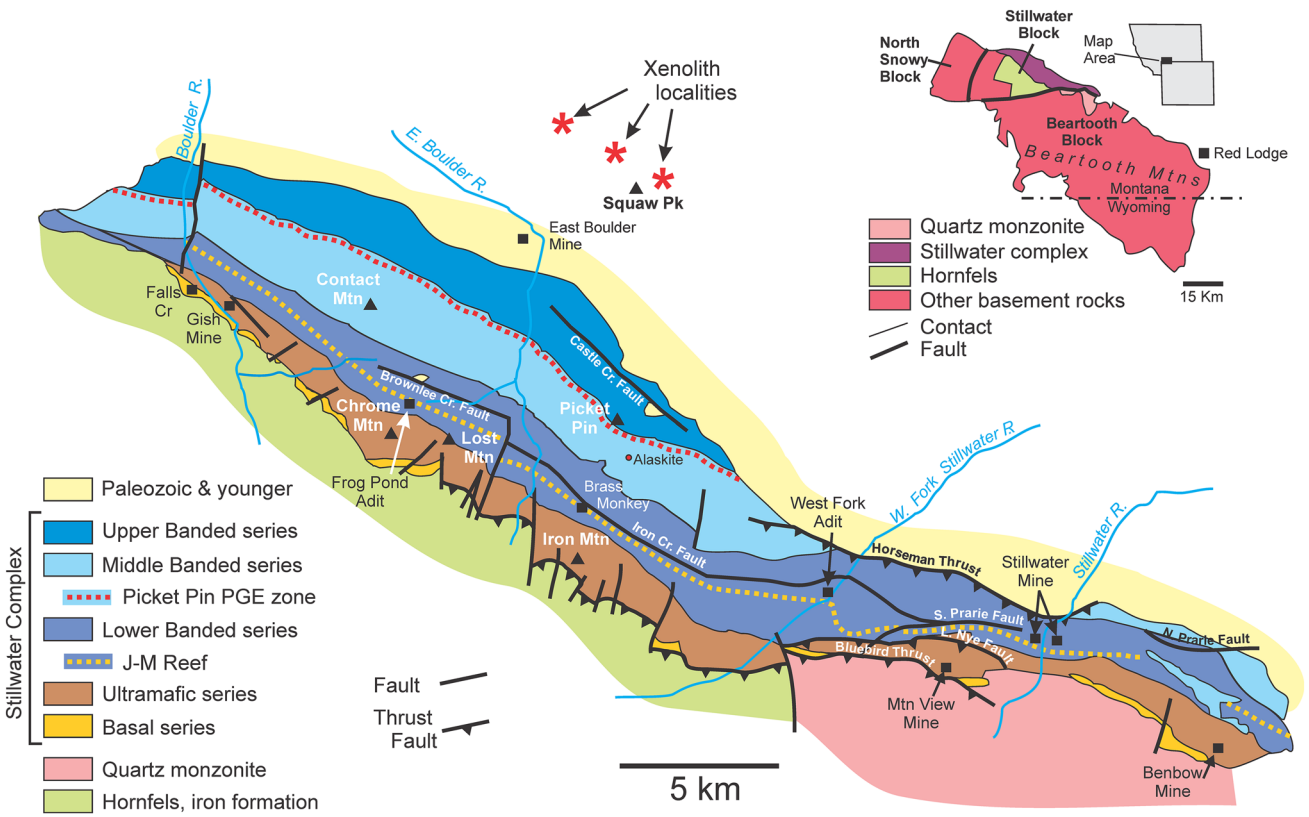

Fig. 1 Geologic map of the Stillwater Complex including the major divisions within the complex and its relative location compared to the surrounding geology

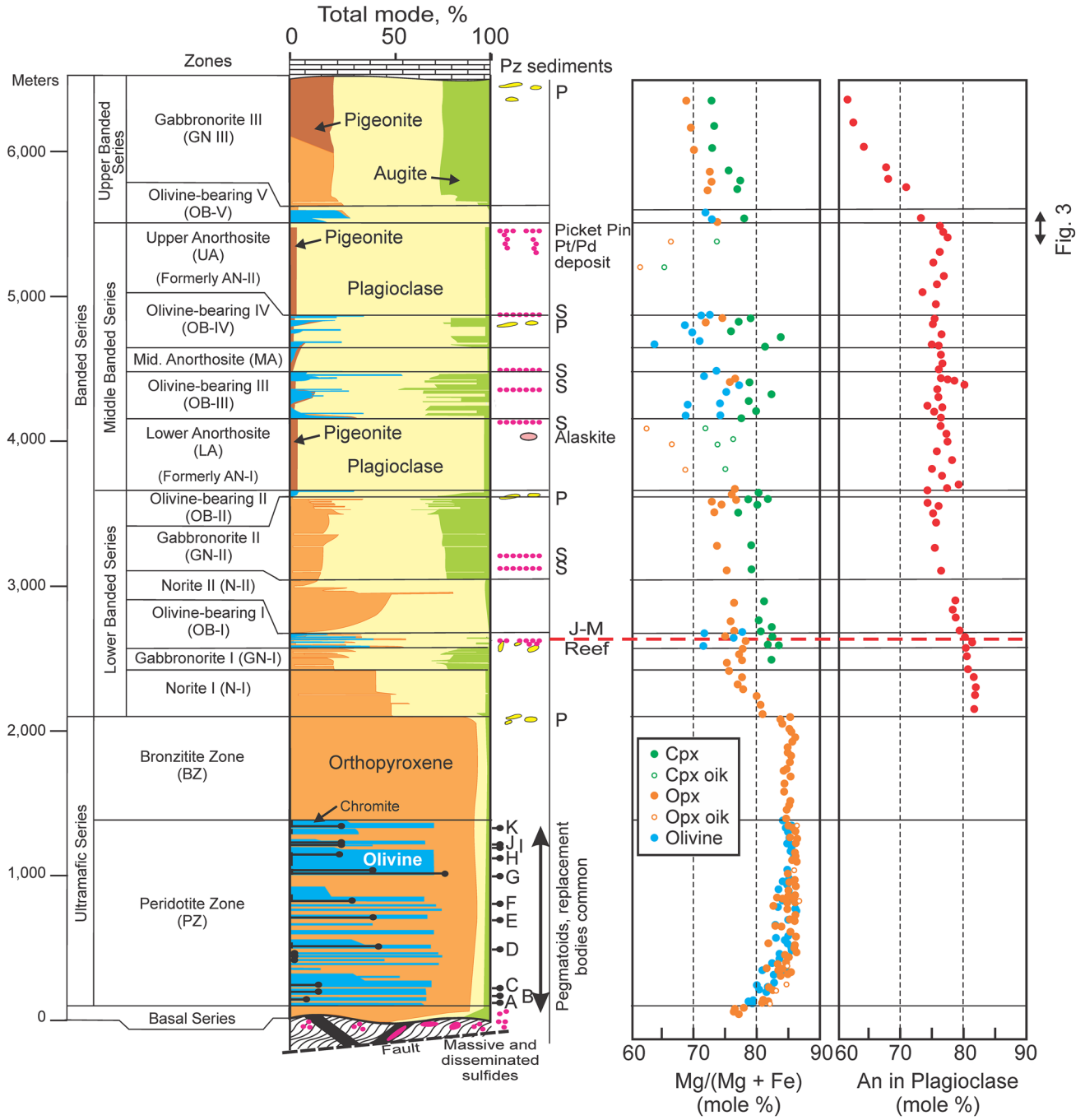

Fig. 2 Major stratigraphic units (formal and informal), mineral modes, and mineral compositional trends as a function of stratigraphic height in the Stillwater Complex. Modal olivine in poikilitic and granular harzburgite from the Ultramafic series is in part schematic, based on average modes. Also shown are the locations of the A through K chromitites (labeled "A"–"K"), zones where pegmatoids and sulfides are common (labeled "P" and "S", respectively), the alaskite body described by Czamanske et al. (1991), and the locations of the J-M reef and the Picket Pin PGE zone (labeled). Modal data after McCallum et al. (1980) and Raedeke and McCallum (1984). The stratigraphic location of the detailed section shown in Fig. 3 is shown marked at the top of the Middle Banded Series

The Basal Series extends from the base of the Stillwater Complex to an average height of 160 m until the start of the Ultramafic Series. The contact with the underlying metasedimentary country rock, altered largely to cordierite–pyroxene hornfels, is locally faulted and cuts across footwall stratigraphic units, suggesting that the complex was emplaced along an unconformity. The Basal Series is composed largely of norite and bronzitite. The contact with the overlying

Ultramafic Series is defined by the appearance of olivine-bearing lithologies. The 1–2 km thick Ultramafic Series is divided into two zones: the peridotite zone, in which the rocks are composed of multiple cyclic sequences of dunites, harzburgites, chromitites and orthopyroxenites, all defined by variable proportions of orthopyroxene, chromite, and olivine, and the Bronzitite zone, which is comprised of mostly uniform composition orthopyroxenite.

The base of the Banded Series is defined by the appearance of abundant plagioclase. This series has been informally divided into three zones: the Lower Banded Series (LBS), the Middle Banded Series (MBS), and the Upper Banded Series (UBS) (McCallum et al. 1980). The LBS extends from about 2200 m to about 3600 m, and is comprised primarily of gabbronorites and norites. This series also contains Olivine-bearing zone I (OB-I) which is marked by the reappearance of olivine-bearing rocks and which contains the J-M Reef, a zone containing economic grades of palladium and platinum hosted in disseminated sulfides. The MBS extends from about 3600 to 5500 m. Much of this series is comprised of three large anorthosite units, the largest up to 600 m thick. The middle anorthosite is the thinnest and is not broken out in the stratigraphic subdivisions of McCallum et al. (1980), who denoted the lower and upper anorthosites Anorthosite subzones I and II, respectively. Boudreau (2016) noted the similarities of the middle anorthosite with the other two and denoted them the Lower, Middle and Upper Anorthosite subzones of the Middle Banded series, consistent with earlier subdivision of Hess (1960), and it is this nomenclature that is used here. Besides plagioclase, the anorthosites contain heterogeneously distributed interstitial to oikocrystic inverted pigeonite, clinopyroxene, magnetite, apatite, and quartz. A zone of lenticular and podiform platinum-group element-bearing disseminated sulfides occurs in the upper part of the Upper Anorthosite subzone (the Picket Pin PGE zone).

Troctolite, more medium-grained anorthosite, and olivine gabbro make up most of the remainder of the Middle Banded series. Unlike the Ultramafic series and the much of the rest of the Banded series, orthopyroxene appears to crystallize late, if at all, in the Middle Banded series and is discussed more below. The Upper Banded Series, in contrast, again returns to norite and gabbronorites above the troctolite unit of Olivine-bearing zone V (OB-V). It is the origin of OB-V that is the subject of this report (Fig. 2) but has implications for the origins of olivine in OB-III and OB-IV.

Two features associated with the MBS and the immediately surrounding rocks have been the subject of several contrasting interpretations. The first is the cause for the reappearance of olivine in the MBS, in OB-II just below the MBS, and in OB-V just above the MBS. The second has to do with the apparent change in the crystallization sequence in the MBS in which opx crystallized late (olivine + plagioclase → olivine + plagioclase + clinopyroxene → plagioclase + clinopyroxene + orthopyroxene) as compared with that elsewhere where orthopyroxene appears early (olivine ± chromite → orthopyroxene → orthopyroxene + plagioclase → orthopyroxene + plagioclase + clinopyroxene). This crystallization sequence is so distinct from those elsewhere in the Stillwater Complex that it has been hypothesized that the composition of its parental magma differed dramatically from that which formed the Lower and Upper Banded series (Raedeke 1982 and Irvine et al. 1983). For example, Irvine et al. (1983) proposed that both magmas were present in the magma chamber but were separate due to their different densities. The troctolite unit of OB-V above the Upper Anorthosite unit was the last expression of this different magma prior to the return to crystallization of norites and gabbronorites similar to those of the Lower Banded Series.

In contrast, Boudreau (2016) noted the abundance of podiform and discordant bodies of replacement troctolite and anorthosite in the Middle Banded series, the compositional similarities of these replacement bodies with the layered olivine-bearing rocks (e.g., Meurer et al. 1997), and the lack of offsets in mineral compositional trends to more primitive compositions. He suggested that a plagioclase + pyroxene mush protolith and/or magma was hydrated with H_2O-bearing vapor by the degassing of the underlying anorthosite mush that stabilized olivine rather than pyroxene through partial melting and silica leaching. It was suggested that the thick anorthosite units were particularly prone to degas large volumes of H_2O owing to their thickness and large volume of evolved interstitial liquid abundance that was not lost early to compaction. The development of troctolite above the anorthosite units was an expected consequence of this degassing as these fluids moved into the hotter overlying pyroxene-bearing mush where it induced partial melting and leached silica and the alkalis. It was suggested that reverse zoning in plagioclase would be an expected consequence of these processes and is the subject of this study.

Petrography

Figure 3 shows a detail of the lithologic units of the uppermost part of the Upper Anorthosite and into the lower part of the overlying Olivine-bearing zone V. The bulk of the ~ 600 m thick Upper Anorthosite unit consists of abundant course-grained plagioclase with < 5 to 20% pyroxene oikocrysts, the latter composed of subequal proportions of a high Ca pyroxene and an inverted pigeonite. While common in the thick anorthosite units of the Middle Banded series, inverted pigeonite does not occur elsewhere in the section until it occurs in the more evolved rocks in

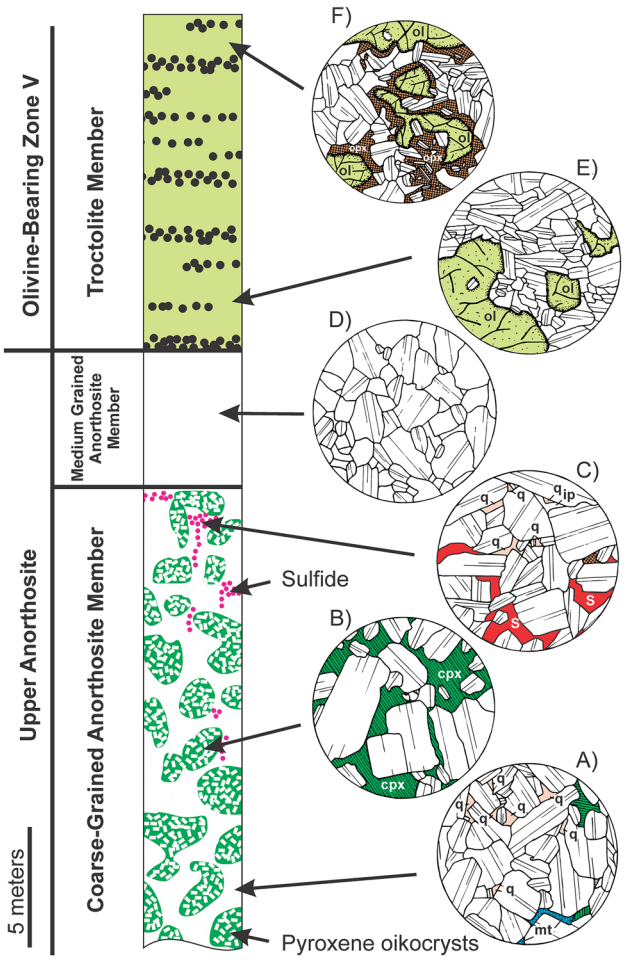

Fig. 3 Detail of the section at the Middle Banded series—Upper Banded series contact. All petrographic sketches are 1 cm in diameter. **a** Plagioclase (showing orientation of albite twins) with minor interstitial augite (green-ruled). **b** Plagioclase enclosed within oikocrysts of augite (green-ruled); also minor quartz (q) and ilmenite (blue-stippled). **c** Interstitial PGE-bearing sulfide (red), quartz (q), and minor pyroxene (brown-cross ruled). **d** Monomineralic anorthosite with well-developed triple junctions of the Medium-Grained Anorthosite member. **e** Troctolite with olivine (pale green) and plagioclase. Olivine may enclose grains of plagioclase. **f** Olivine rimmed with low-Ca pyroxene (brown-cross ruled). The amount of pyroxene increases up-section within the Troctolite member. Redrawn after Boudreau and McCallum (1986)

the upper part of Gabbronorite zone III at the top of the exposed portion of the complex.

A thin, 5–10 m thick medium-grained anorthosite composed almost entirely of plagioclase defines the top of the Upper Anorthosite. Occurring in the upper ~ 150 m of the upper anorthosite but below this medium-grained unit are podiform and discordant pipes of disseminated sulfide mineralization with modest PGE enrichments (~ 1 ppm each Pt and Pd, maximum), known as the Picket Pin PGE zone (Boudreau and McCallum 1985, 1986).

Fig. 4 Example of the "wispy layered" troctolite of Olivine-bearing zone V (OB-V) at the base of the Upper Banded series. The troctolite above the Lower Anorthosite zone at the base of the Middle Banded series is similar

The top of the Upper Anorthosite marks the base of Olivine-bearing zone V (OB-V) and the start of the Upper Banded series. Troctolite and lesser anorthosite are the main lithologies of this section. The lower part of OB-V is composed almost entirely of plagioclase and olivine with modal variations producing a discontinuous "wispy" layering in outcrop (Fig. 4). Olivine grains vary in size from several mm to ~ 1.0 cm. The olivine has an irregular "amoeboidal" shape with a poikilitic texture and contain small, tabular to rounded plagioclase chadacrysts. The non-chadacrystic plagioclase is primarily euhedral to subhedral and of a similar to larger size as the chadacrysts (approximately a millimeter in length). With increasing height, orthopyroxene becomes more abundant, occurring as an intersititial-oikocrystic mineral enclosing plagioclase and as a rimming mineral to olivine. Several samples contain a green hornblende, typically found associated with plagioclase chadacrysts in an olivine host (Fig. 5).

Materials and methods

Polished thin sections of fresher troctolite samples from drillcores through Olivine-bearing zone V (Boudreau and McCallum 1986) were used in the analysis. Petrographic identification of unaltered grains of plagioclase next to or within grains of olivine, orthopyroxene, or other grains of plagioclase were marked on photomicrographs of the thin sections.

The specified grains were then analyzed with a Cameca Camebax electron-microprobe to determine the composition of specific points on the marked grains. Standard analytical conditions were 15 keV acceleration voltage,

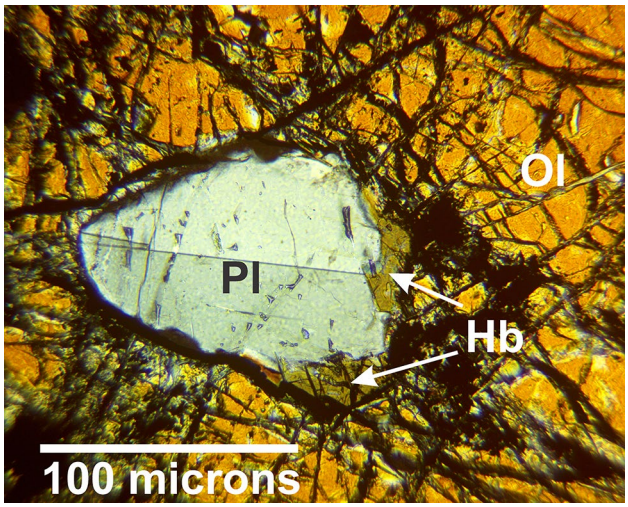

Fig. 5 Photomicrograph of plagioclase and hornblende inclusions in partly altered olivine, sample CM1–87

15 nanoamp beam current, and a beam defocused to 10 microns. Natural feldspars were used as standards. A Phi-Rho-Z correction routine (PROZA96, Bastin et al. 1996) was used to correct the data. The grains were analyzed in core/rim pairs, with one point on the edge of a plagioclase grain and the other point towards the center. Several core/rim analyses were conducted for each grain, and approximately a dozen grains were analyzed for each thin section. The microprobe was also used to analyze a straight line of 19 evenly spaced points across the grain shown in Fig. 5.

Results

In total, 99 core/rim pairs from 5 samples from Olivine Bearing zone V were analyzed with the electron microprobe; results are shown in the histograms in Figs. 6 and 7. Typical analyses are shown in Table 1 and additional data is presented in the supplemental data file. Eighty-three pairs were reversely zoned, and 16 were normally zoned. The most negative difference was −8.3, the most positive was 4.3, but the majority of pairs were clustered between −6 and 1. The average difference was −2.8. Core points had an average An number of 77.8, typical for other plagioclase from the MBS (McCallum et al. 1980). Rim points had an average An number of 80.7. All of the averages and highest and lowest values are shown in Table 1. The transect across the grain enclosed in olivine is shown in Fig. 8. The core analyses tend to be erratic but overall less anorthitic than either rim.

There is no marked difference between the An numbers of plagioclase grains bordering other plagioclase grains versus bordering olivine or (in samples where present) orthopyroxene. All have similar reversely zoned An averages: −2.6 for pl–pl grains, −2.7 for pl–ol grains, and −3.2 for pl–opx. All of the thin sections analyzed generally follow the same pattern. No one sample had a

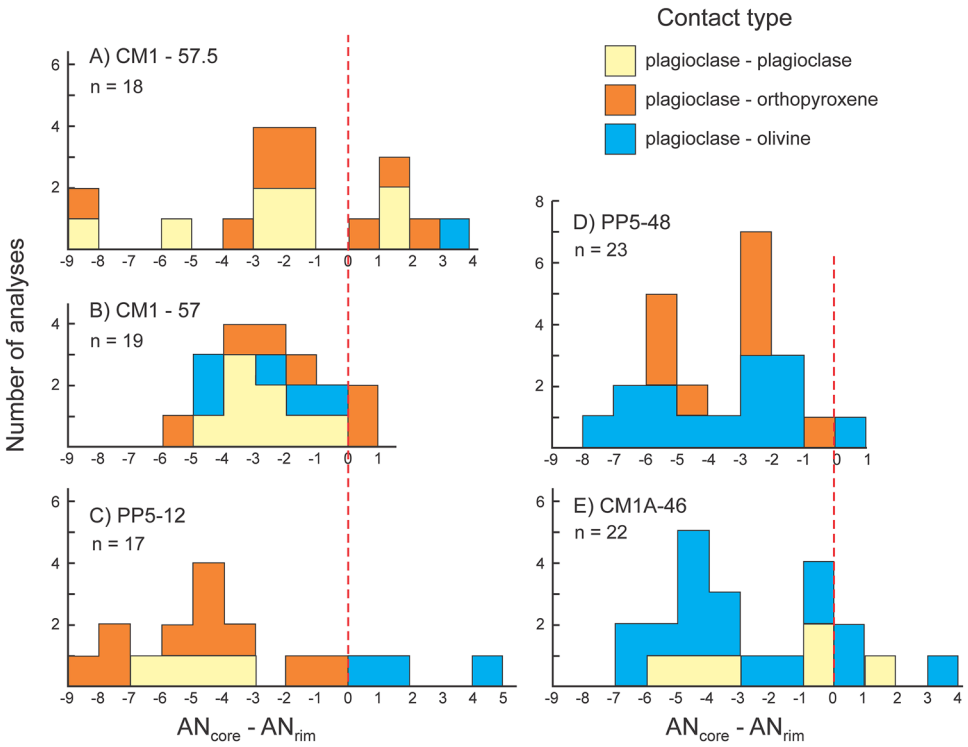

Fig. 6 Histograms for plagioclase core-rim analyses for each sample analyzed. The difference between the An numbers of core-rim pairs lies along the *x*-axis, while the *y*-axis shows the number of pairs with the observed differences. Colors denote the type of adjacent mineral for the rim analysis

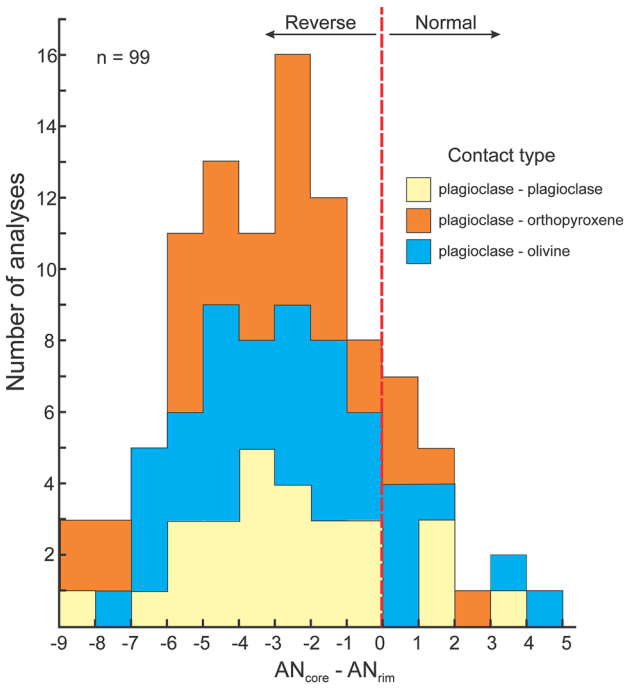

Fig. 7 Histogram of plagioclase core-rim analysis for all five samples. Colors denote the type of adjacent mineral for the rim analysis

substantial difference in the ratio of reversely zoned points to normally zoned points; all had a few normally zoned but a majority reversely zoned.

It is noted that, with the exception of one outlying core (Table 2), the average rim An of 80.7 is not seen in any core compositions anywhere in the upper part of Middle Banded and Upper Banded series (McCallum et al. 1980). Indeed, the Upper Banded series plagioclase show a marked trend of decreasing An numbers with stratigraphic height above OB-V. One has to go down to the lower parts of the Lower Banded series to find plagioclase core compositions as An-rich as the OB-V rims (Fig. 2).

The amphibole analysis of a grain from CM1–87 is shown in Table 3. The grain is associated with plagioclase trapped within olivine (Fig. 5). The amphibole is a pargasitic (sodium-rich) green hornblende. It has a calculated hornblende-plagioclase equilibration temperature (893 °C) and pressure (1.5 kbar) that is constant with a high temperature, low pressure formation of the hornblende and the host olivine.

Discussion

Conventional cumulus theory suggests that cumulus minerals will continue to grow by postcumulus overgrowth during solidification of the pore liquid (Wager et al. 1960). Normal zoning is expected for plagioclase crystallizing from a magma undergoing crystallization along a closed system liquid line of descent. For plagioclase accumulating in a mush zone on the floor of the magma chamber, closed system crystallization of interstitial liquid and the slow solid state diffusion in plagioclase should lead to modest normal zoning, the enrichment depending on the amount of residual liquid present (but see below). For example, plagioclase from the Rum intrusion can have typical normal zoning of about 20% An content (O'Driscoll et al. 2009). In contrast, normal zoning is absent for the majority of plagioclase in OB-V.

Other examples of reverse zoning in igneous intrusions have been explained through a variety of orthomagmatic models. For example, Morse and Nolan (1984) suggested that reverse zoning can be caused by the re-equilibration effects of adjacent Al-bearing augite. This would not be effective in troctolite of OB-V owing to the paucity of pyroxene, particularly Ca-rich pyroxene, in most samples.

Table 1 Examples of plagioclase core and rim analyses

Sample	CM1-57		CM1A-46		CM1-57.5	
Contact	pl–opx		pl–ol		pl–pl	
	Core	Rim	Core	Rim	Core	Rim
SiO_2	48.2	47.7	48.3	47.2	48.5	46.9
Al_2O_3	33.8	33.9	33.4	33.9	33.2	34.1
FeO	na	na	0.35	0.34	0.41	0.31
MgO	na	na	nd	nd	0.02	0.01
CaO	15.9	16.2	16.1	16.2	15.3	16.4
Na_2O	2.53	2.32	2.63	2.24	1.98	1.67
K_2O	nd	nd	0.02	nd	0.07	0.05
Total	100.5	100.1	100.8	100.2	100.1	99.1
An#	77.4	79.2	77.2	77.9	75.8	81.1
$Si+Al+Fe^{3+}$	4.00	4.00	3.99	1.01	4.01	4.00
Na + Ca + K	1.00	1.00	3.99	1.01	0.99	1.00

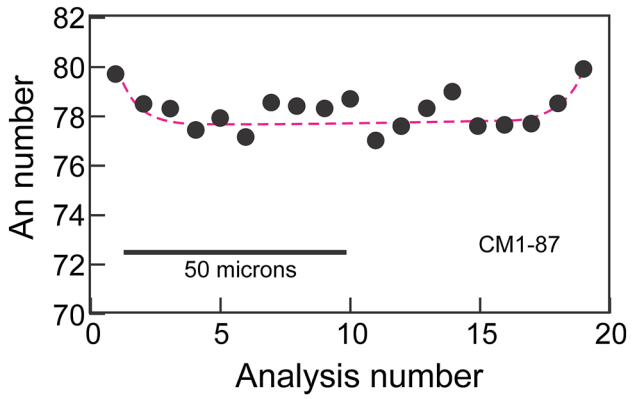

Fig. 8 Compositional profile of the grain from CM1–87 shown in Fig. 5, in which each point represents the An number of a point of analysis, with points spread equidistantly across the grain

Table 2 Plagioclase composition summary

Average core	77.8 ($n=99$)
Lowest core	73.1
Highest core	81.9
Average rim	80.7
Lowest rim	71.2
Highest rim	86.3
Average difference	−2.83
pl–pl average	−2.62
pl–ol average	−2.67
pl–opx average	−3.16
Largest negative difference	−8.34
Largest positive difference	4.31

Table 3 Amphibole analysis, sample CM1–87

	Wt%	Structural formulae[a]
SiO_2	44.6	6.33
TiO_2	1.81	1.93
Al_2O_3	13.2	1.67 (IV), 0.541 (VI)
FeO	8.83	0.585 (Fe^{2+}), 0.464 (Fe^{3+})
MnO	nd	0.00
MgO	15.2	3.27
CaO	11.8	1.80
K_2O	0.75	0.14
Na_2O	2.00	0.55
F	0.09	0.04
Cl	0.23	0.06
H_2O	1.51	1.90
Total	100.0	17.5
Calculation scheme		
(Ca + Na) (B)	2.000	
Na (B)	0.205	
(Na + K) (A)	0.481	
Mg/(Mg + Fe^{2+})	0.846	
Fe^{3+}/(Fe^{3+}+Al^{vi})	0.461	
Sum of S2	13.00	
Name: Hornblende		
Temperature[b]	893 °C	
Pressure[b]	1.52 kbar	

[a]Structural formulae and calculation scheme calculated by the excel spreadsheet "Probe-Amph" distributed for free by Andy Tindel, Centre for Earth, Planetary, Space and Astronomical Research, The Open University, UK

[b]Temperature and Pressure from the plagioclase-hornblende geothermometer of Holland and Blundy (1994) with modifications of Anderson (1996) using average plagioclase rim compositions of Table 1 and calculated using the excel spreadsheet "RiMG069_hbld_plag_thermo-jla.xls", distributed for free by Lawford Anderson, University of Southern California

Plagioclase in the Skaergaard intrusion, where the cumulus paradigm was developed, commonly show reverse, oscillatory and skeletal zoning, and has been attributed to supercooled crystallization (Maaløe 1987; Mathison 1987). Even if supercooling were true for core compositions, one would still expect the rims to tend towards normal zoning once the grains were trapped within the crystal pile. Toplis et al. (1980) noted that the plagioclase rim compositions are approximately constant in composition from the Lower Zone to the lower Middle Zone of the Skaergaard intrusion, which they attribute to buffering by convection of an interstitial liquid crystallizing through a density maximum.

Hayes et al. (2017) explained a modest reverse zoning of plagioclase (~2 mol%, similar to that seen here) in the Main Zone of the Bushveld Complex by the downward percolation of a more primitive magma through the crystal mush to produce the reverse-zoning. If this orthomagmatic model were true for the plagioclase of this study, then one would expect to see plagioclase crystallizing with core An numbers that are at least as An-rich as the most primitive OB-V rim values somewhere in the overlying stratigraphy. Instead, as noted above the core compositions become less anorthitic with stratigraphic height throughout the Upper Banded series (McCallum et al. 1980; see also Fig. 2).

The presence of reversely zoned plagioclase grains is observed elsewhere in the Stillwater Complex. Rounded, reversely zoned plagioclase are characteristic of the olivine-bearing rocks of OB-I, the host zone of the PGE-rich J-M Reef (Barnes and Naldrett 1986; Boudreau 1988). Barnes and Naldrett (1986) suggested the reverse zoning was the result of a magma mixing scheme. In contrast, Boudreau (1988, 2016) noted the lack of stratigraphic offsets to more An-rich compositions across the J-M Reef section and instead suggested that the reversely zoned plagioclase (and the presence of olivine as well) was the result of volatile fluid fluxing and incongruent partial melting of a gabbronorite and norite protolith. In regard to the hydromagmatic model,

Maier et al. (2016) noted that reversely zoned plagioclase is typical of plagioclase in the UG3 section of the Bushveld Complex. Similarly, Maier (1995) noted rounded, reversely zoned plagioclase entrained in olivine oikocrysts in Bushveld anorthosite similar to the observed in OB-V. In both cases a hydromagmatic model of partial melting or resorption of plagioclase by an interstitial liquid enriched in H_2O was proposed.

There are two ways by which the addition of H_2O can produce reverse zoning in plagioclase. First, illustrated in Fig. 9, the addition of H_2O to the plagioclase system leads to a lowering of the plagioclase solid solution loop to lower temperatures (e.g., Yoder and Tilley 1962; Schmidt et al. 2008). Hydration of a plagioclase-liquid mixture at a constant temperature and pressure will shift both the liquid and the plagioclase to more anorthitic compositions, resulting in a reversely zoned plagioclase. It is also noted that continued cooling and crystallization of the hydrated system should then crystallize a normally zoned plagioclase unless the hydrated melt is lost. However, this could account for some of the observed weakly but normally zoned plagioclase.

The second fluid-mediated mechanism involves a migrating aqueous fluid (aq) that becomes silica-undersaturated as it moves into hotter rocks, leaching SiO_2, alkalis, and other elements as it does so:

$$\underset{\text{aq}}{H^+} + \underset{\text{aq}}{2H_2O} + \underset{\text{plagioclase}}{(Ca, Na)(Al, Si)\left(AlSi_2O_8\right)} \rightarrow \underset{\text{aq}}{Na^+} + \underset{\text{aq}}{H_4SiO_4} + \underset{\text{plagioclase}}{CaAl_2Si_2O_8}\,. \quad (1)$$

Experimental studies of silica solubility in aqueous fluids at pressure applicable to the Stillwater Complex (2–3 kbar) are typically limited to $T \leq 700$ °C (c.f. summary by Sverjensky et al. 2014). Given that the Stillwater fluids could be interacting with a mush that is just below its liquidus, one needs to extrapolate to these higher temperatures where other aqueous species can become increasingly important but poorly explored. For example, the experimental work by Newton and Manning (2000) suggest that modest amounts of NaCl in a hydrous fluid ($X_{NaCl} \cong 0.1$) can cause a roughly 50% increase in SiO_2 solubility compared to NaCl-absent aqueous fluids at 700 °C and 2 kbar. These experiments show the importance of Cl–Na complexing in enhancing silica solubility at high temperatures that is not significant at lower temperatures. Evidence for a Stillwater fluid Cl component is seen in the Cl concentrations in apatite that range as high as 50 mol% chlorapatite in OB-V (Boudreau and McCallum 1989) as well as the Cl in amphibole reported here (Table 3).

The prevalence of reversely zoned grains relative to normally zoned grains is consistent with silica and sodium loss from pre-existing plagioclase. There is also no evidence of plagioclase core compositions being reset to more primitive, An-rich compositions either in OB-V or any of the overlying units. Instead, the plagioclase core compositional trends continue fractionation trends typical of the UBS rocks in general. The preservation of the green hornblende associated with plagioclase enclosed in olivine also supports a hydration hypothesis.

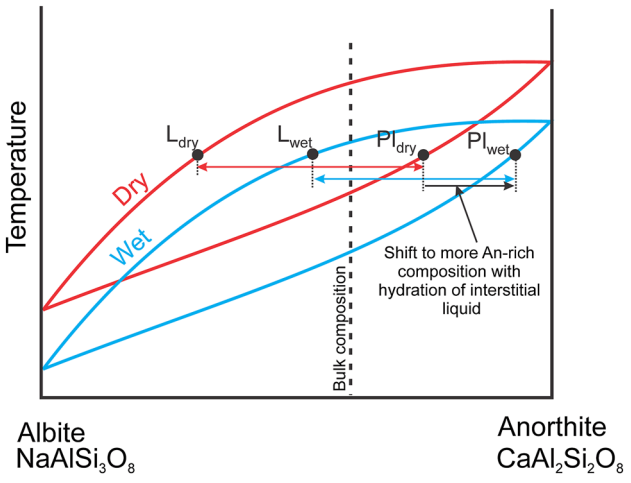

Fig. 9 The shift in the solid solution loop for plagioclase between pure albite and pure anorthite for both dry (red) and wet (blue) conditions. Generalized after Yoder and Tilley (1962); see text for details

This also has implications for the reappearance of olivine in OB-V. Raedeke (1982) and Irvine et al. (1983) have proposed orthomagmatic models in which either an olivine-saturated magma was introduced into the partly crystallized magma chamber or that mixing of the resident magma with an anorthositic liquid produced an olivine-saturated hybrid liquid. As noted above, the lack of any compositional offset in the stratigraphic trends of minerals compositions, particularly plagioclase, would suggest that these mixing schemes would have to have rather fortuitous compositional characteristics to match the fractionation trends of the resident magma. Instead, the silica loss of reaction (1) can also convert pyroxene to olivine by an incongruent dissolution reaction:

$$\underset{\text{aq}}{2H_2O} + \underset{\text{opx}}{Mg_2Si_2O_6} \rightarrow \underset{\text{aq}}{H_4SiO_4} + \underset{\text{olivine}}{Mg_2SiO_4}\,. \quad (2)$$

The model proposed here is similar to that proposed by Meurer et al. (1997) to explain transgressive zoned anorthosite-troctolite bodies developed in (gabbro)norite rocks of the Middle Banded Series. They noted that aqueous fluids moving into hotter parts of the crystal mush will become undersaturated in Si (Fig. 10a) such that the fluid

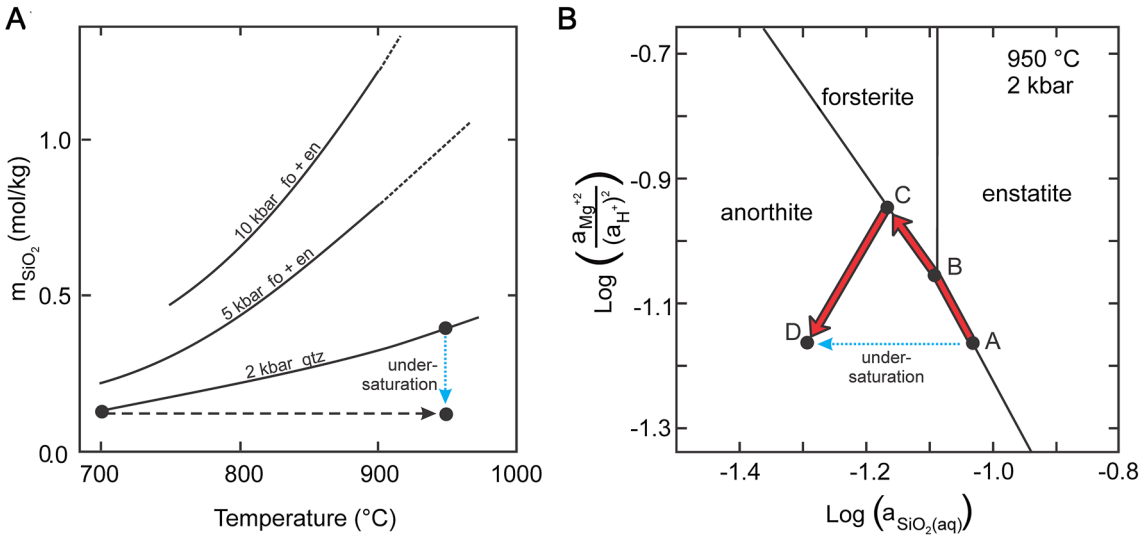

Fig. 10 **a** Solubility of SiO_2 in fluid saturated in quartz in SiO_2-H_2O fluids (labeled "qtz") and for fluids buffered by enstatite + forsterite (labeled "fo + en"), all at pressures noted. Owing to the increasing silica content of the fluid of the various buffers with increasing temperature, heating of fluids will result in the fluid to become increasingly silica-undersatured as shown schematically for the quartz saturation curve. The forsterite-enstatite buffered curves are after Mysen et al. (2013; dashed portions are extrapolated), and the silica solubility curve and the activity diagram are as calculated by the program CHNOSZ (Dick 2019) an update of the SUPCRT92 program (Johnson et al. 1992). **b** Activity diagram showing the stability fields of the anorthite, enstatite, and forsterite as a function of the activity ratio $a_{Mg^{2+}}/a^2_{H^+}$ and $a_{SiO_2(aq)}$, all reactions balanced on H_2O in formation reactions at 950 °C and 2 kbar. Lowering the activity of silica in a fluid initially saturated in enstatite + anorthite (point "A") moves the fluid to be within the anorthite-alone field (point "D"). The red arrow shows a reaction path as the silica-poor fluid reacts with the anorthite + enstatite protolith assemblage at point "A" to produce troctolite (path B–C) at low fluid/rock mass ratios and anorthosite (path C–D) at higher fluid/rock mass ratios. Activity diagram calculated using the program CHNOSZ (Dick, 2019) with ausing typical Upper Banded series mineral compositions reported by Raedeke (1982) and activities calculated by the online MELTS supplemental calculator (http://melts.ofm-research.org/CalcForms/index.html): $a_{en} = 0.47$, $a_{ol} = 0.62$, and $a_{an} = 0.80$. Additional aqueous activities set as follows: $\log a_{Ca^{2+}} = -1.0$; $\log a_{Al(OH)_3} = -2.4$, all other aqueous species $\log a = 0.0$ See supplemental data for additional assumptions and a copy of the CHNOSZ script used to compute the activity diagram

moves into an anorthite-alone field as shown in the activity diagram of Fig. 10b. Reaction of this fluid with a norite host results in incongruent dissolution of pyroxene to olivine. With continued fluid inflow, the olivine eventually dissolves leaving a residual anorthosite. The final reaction sequence is norite (protolith) → troctolite → anorthosite. A similar model was suggest by McBirney and Sonnenthal (1990) and Sonnenthal (1992) to explain discordant anorthosite bodies in the Skaergaard intrusion. For the rocks of OB-V, it is proposed that degassing of the underlying Upper Anorthosite was the main source of the fluid affecting the overlying rocks.

The origin of the thick anorthosite units of the Middle Banded series is uncertain. McCallum et al. (1980) suggested that they represent plagioclase that failed to accumulate on the floor of the chamber during crystallization of the Bronzitite zone of the Ultramafic series whereas Czamanske and Bohlen (1990) suggested that they may have intruded as a plagioclase-pyric mush. Whatever their origin, the lack of stratigraphic variability in the average plagioclase composition, the unusually large grain size relative to plagioclase elsewhere in the complex, complex plagioclase zoning and extensive normal zoning in the pyroxene oikocrysts (McCallum et al. 1980; Czamanske and Scheidle 1985; Gitlin et al. 1985) all have been used to support the notion these rocks initially formed as thick, plagioclase-rich mushes.

Previous workers have suggested that there was very little trapped liquid in the Middle Banded series anorthosites owing to the low incompatible element concentrations, and thus some have suggested that the rocks started out as "adcumulates" (e.g., Salpas et al. 1983). However, as summarized by Boudreau (2016), the trace elements are only part of the story. With the exception of the thin, almost pure anorthosite at the top of the Upper Anorthosite (the Medium-Grained Anorthosite member of Fig. 3), the anorthosites are heterogeneously composed of up to 20% large pyroxene (cpx and inverted pigeonite) oikocrysts that are compositionally normally zoned, with quartz, apatite, and magnetite are locally abundant away from these oikocryst-rich regions (Fig. 3a, b). It is otherwise noted that interstitial to poikilitic pigeonite and magnetite do not again become common until pigeonite gabbros appear in the upper part of the Gabbronorite zone III at the very top of the complex. Furthermore, while most bulk rock REE plots of the thick anorthosites show a pronounced positive Eu anomaly expected from the modally dominant

plagioclase, samples with a low abundance of pyroxene can have a flat to even slightly negative Eu anomaly.

Boudreau (2016) suggested that the anorthosites originally started with 30–40% interstitial liquid. Crystallization of this pore liquid produced the large, zoned pyroxene and later magnetite oikocrysts that displaced the increasingly evolved pore liquid. Some of this enriched residual liquid eventually crystallized the locally abundant quartz and apatite. Most, however, was eventually lost, either through compaction owing to the increasing weight of the anorthosite solid assemblage with crystallization of the interstitial pyroxene and magnetite as well as the weight of the rocks above the anorthosites, or simply because the residual liquid evolved to a low density liquid that was advected away. The rocks with negative Eu anomalies were proposed to represent pathways by which this enriched liquid was lost. It was also suggested that "alaskite" body described by Czamanske et al. (1991) may have formed from this late liquid fraction that was lost from the anorthosite.

Presumably at some time during crystallization of the interstitial liquid (and prior to the last residual liqud being lost) the liquid became vapor-saturated. The amount of vapor released could have been substantial: if the mush was initially comprised of 30–40% liquid with 1.0 wt% H_2O, then on degassing the ~ 600 m thick Upper Anorthosite could exsolved enough water to produce a layer of water about 5–7 m thick. In contrast, it is suggested that the rocks above and below the thick anorthosites initially crystallize norite and gabbronorite comprised of plagioclase + relatively more Mg-rich pyroxenes typical of those that make up most of the Banded series away from the thick anorthosite units. This, and the paucity of late-crystallizing minerals in the (gabbro) norite implies that these rocks had a low residual porosity and degassed a proportionally smaller volumes of vapor.

A MELTS model illustrating the effect of the isothermal addition of H_2O to an initially dry, partly molten norite is shown in Fig. 11. It is seen that addition as little as 0.7 wt% H_2O can convert a norite into a troctolite by incongruent hydration melting. A similar model calculation for the hydration of a partially molten gabbronorite was presented by Boudreau (2016), and illustrates that a similarly small amount of H_2O can convert a gabbronorite into an olivine gabbro typical of the Middle Banded series. Mathez and Kinzler (2017) have shown experimentally that the addition of H_2O to a partly crystallized liquid saturated in plagioclase and two pyroxenes can produce a plagioclase + olivine -saturated liquid.

The combined thickness of the olivine-bearing rocks of OB-III and OB-IV of the Middle Banded series and OB-V of the overlying Upper Banded series is roughly half the stratigraphic thickness of the three thick anorthosites of the Middle Banded series. If the anorthosites exsolved 1 wt% H_2O that was all added to the overlying norite or gabbronorite

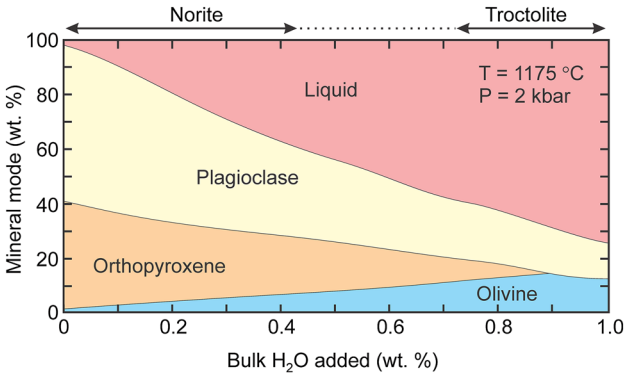

Fig. 11 A MELTS Excel (Gualda and Ghiorso 2015) calculation on the modal changes of a partially molten norite (plagioclase + orthopyroxene + liquid) with addition of H_2O at 1175 °C and 2 kbar pressure. The initial dry bulk composition is that of a typical Bushveld norite (Eales et al. 1986, Table 1 analysis 6). The phase assemblages are calculated as a function of water added to this initial dry composition

protolith, this would be equivalent to the addition of 2 wt% the protolith, more than enough to account for the olivine in these rocks by incongruent melting.

A petrogenetic model is illustrated in Fig. 12. The initial geometry of the system is a thick homogenous anorthosite mush containing up to 40% of a relatively evolved silicate liquid, overlain by what was initially a norite or gabbronorite mush (Fig. 12a), the latter being largely solid owing to a low residual porosity. As the interstitial liquid in the anorthosite cools and crystallizes by heat loss out from the base, it becomes vapor saturated. Although this vapor could move into hotter magma and lead to expansion of the olivine phase field, this is considered less likely owing to the textural observation that the olivine is typically irregular/amoeboidal rather than the equant/euhedral shape one might expect if the olivine grew in a liquid-rich environment. The texture is more associated with the replacement troctolite bodies found locally throughout the Banded series.

As the vapor moves upward into hotter mush, it reacts to remain in chemical equilibrium with the solid assemblage by two main reactions: (1) hydration of interstitial liquid leads to incongruent melting producing olivine after pyroxene. Loss of the melt produced by this melting event allows the olivine to be preserved as the system continues to cool and resolidify. (2) Heating of the fluid will also drive the fluid to be undersaturated in silica, and the reactive fluid further leaches silica to produce olivine and reverse-zoned plagioclase to produce troctolite (Fig. 12b).

It has been suggested by reviewers of this manuscript that if the olivine replaced pyroxene by an incongruent melting or dissolution reaction event, it should form rims of olivine on the pyroxene. That is, the replacement should be the reverse of the commonly observed peritectic reaction observed in crystallizing magmas where orthopyroxene will

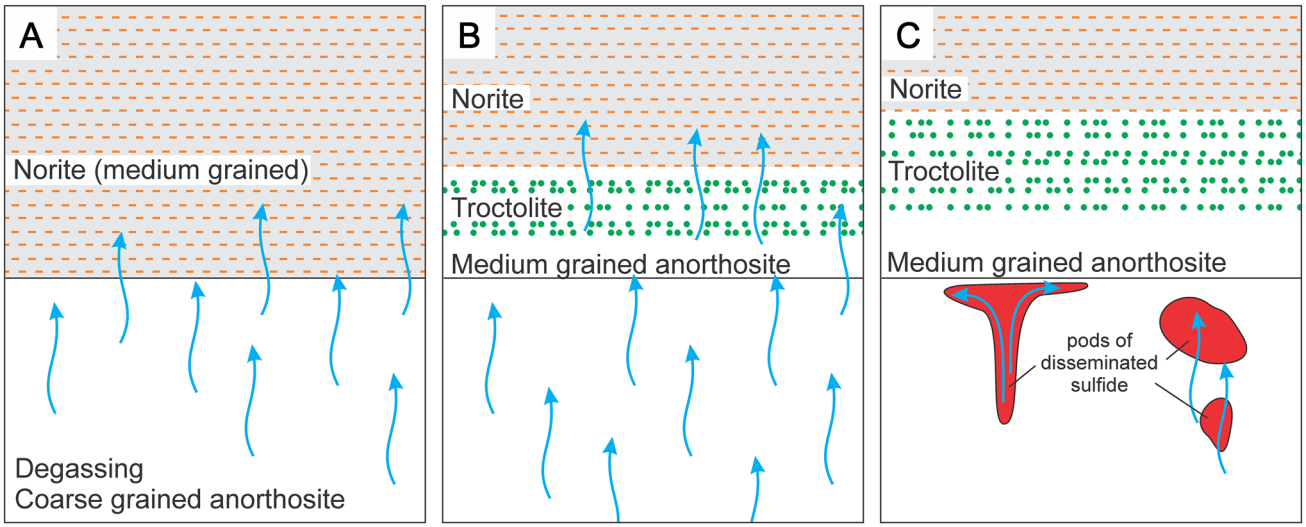

Fig. 12 A degassing model for the formation of the Medium-Grained Anorthosite member and overlying troctolite of Olivine-bearing zone V by hydration melting and vapor leaching during degassing of the underlying coarse-grained anorthosite member of the Upper Anorthosite unit of the Middle Banded series. See text for discussion

rim earlier formed olivine. Evidence for the replacement mechanism is seen in the Middle Banded series where discordant troctolite locally replaces a gabbroic protolith. The early stage of replacement forms what Hess (1960) called "egg-like" features, with olivine surrounded by cm-scale zones of plagioclase devoid of pyroxene (Boudreau 2016; see Fig. S1 in supplemental data file). This olivine gabbro can transition to a discordant troctolite with complete loss of pyroxene. In both rocks the olivine has the same composition and has an amoeboidal shape with abundant plagioclase inclusions (Meurer et al. 1997). The textural evidence shows that olivine grow by nucleating new grains that grow by the dissolution of surrounding pyroxene to produce the pronounced anorthositic selvages in the olivine gabbro where the replacement is only partial. The same kind of reaction relationship in which olivine grow as a separate grains rather than rimming the dissolving/melting pyroxene is also seen in the pillow troctolite that comprises Olivine-bearing zone II (Boudreau 2016). It is evident that the dissolving face of the pyroxene is not a favorable site for olivine nucleation when the net mass of solids is decreasing. Once the hydration/vapor leaching event has passed, however, the crystallization of any residual melt can form the typical peritectic orthopyroxene reaction rims on olivine, as seen in the upper parts of OB-V just below the overlying norite unit at the base of GN-III.

With continued melting and fluid influx, olivine itself melts or dissolves leaving only plagioclase, resulting in the mono-mineralic medium-grained anorthosite member at the very top of the coarse-grained anorthosite member. Towards the end of the solidification of the anorthosite, S-bearing vapor becomes impeded by this low-porosity anorthosite and precipitates disseminate PGE-bearing sulfide in pods, pipes, and lenses in the upper part of the coarse grained anorthosite member of the Upper Anorthosite zone (Fig. 12c).

The lack of hornblende outside of the small amounts seen trapped within the secondary olivine suggest that the vapor degassing, melting and leaching event was short lived. It is suggested that falling f(H_2O) while the rocks were still hot destabilized any high temperature ($\gtrsim$900 °C) amphibole that may have formed during the main leaching event and not protected by being enclosed in olivine.

There are a number of features of Olivine-bearing zone V that have been attributed to current activity, including the wispy layering and suggestions of cut and fill structures seen in the troctolite immediately above the two thickest anorthosite units, and soft-sediment-like layer deformation containing rolled "snowball" pyroxene oikocrysts seen in the norites just above the troctolite unit of OB-V (e.g., McCallum 1996). In the model here, these are interpreted to reflect the increase in the silicate liquid fraction during hydration melting and shear instabilities in the crystal mush as compaction and interstitial liquid convection drives loss of the melt rather than true sedimentary structures.

This model is a modification of an earlier model proposed by Boudreau and McCallum (1992), who suggested that the monomineralic anorthosite zone at the top of AN II can be attributed to infiltration of interstitial silicate liquids from AN II, saturated in plagioclase alone, that were displaced upward into the troctolite during modest compaction of AN II and redissolved olivine. Their model had the troctolite as pre-existing unit, where it is proposed here that the formation of the Medium-grained Anorthosite member of the Upper Anorthosite zone and the overlying troctolite

of Olivine-bearing zone V are the result of the same partial melting/vapor leaching processes described here.

In the rocks above Olivine-bearing zone V the effect of the degassing anorthosite decreased with stratigraphic height as the vapor re-equilibrated with the host assemblage or was otherwise lost and the rocks returned to the plagioclase-pyroxene assemblages typical of the Lower Banded series. In contrast, the gabbros and norites of the Middle Banded series, being interlayered with the Lower and Middle Anorthosites zones were unable to escape the effects of the degassing of these units. The result is the abundance of troctolite and olivine gabbro typical of the Middle Banded series.

Conclusions

The prevalence of reversely zoned core-rim pairs indicates the existence of silica-undersaturated fluid movement through the cooling Stillwater magma, leading to the formation of olivine after pyroxene and resultant troctolite and olivine gabbro by hydration melting and metasomatic reactions with plagioclase-pyroxene protoliths above the thick anorthosites of the Middle Banded series. The model implies that stratigraphic sections with apparently different crystallization sequences need not be the result of the injection of either more primitive magmas or magmas with a different liquid line of descent. Instead these modal and mineral changes can be produced by processes that occur during the crystallization of a single, monogenetic magma.

Reverse-zoned plagioclase is not uncommon in layered intrusions, and the processes discussed here in regard to leaching by high temperature fluids may be more common than generally recognized. It is suggested that these fluids can play much more subtle effects on crystallization behavior such as the formation of modal layering as described by the constitutional zone refining model of McBirney (1987).

Finally, this work illustrated the need for mineral solubility studies at temperatures appropriate for the solidification of mafic magmas ($T \gtrsim 900$–1000 °C) at upper crustal pressures. The work of Newton and Manning (2000, 2016) illustrate the importance of Cl complexing on silica solubility under these conditions that are not evident by extrapolation from lower temperature studies. The role of fluids as solutions and not just a gas phase that is extensively studied in the granite literature needs to be expanded to include ultramafic–mafic rocks.

Acknowledgements This work was supported by donated microprobe time at the Duke University Electron Microprobe Lab. Special thanks for the careful reviews by Rais Latypov and Chris Ballhaus that led to considerable improvement in the manuscript.

References

Anderson JL (1996) Status of thermobarometry in granitic batholiths. Trans R Soc Edinb Earth Sci 87:125–138

Barnes SJ, Naldrett AJ (1986) Geochemistry of the J-M reef of the Stillwater Complex, Minneapolis Adit area II. Silicate mineral chemistry and petrogenesis. J Petrol 27:791–825

Bastin GF, Dijkstra JM, Heijliger HJM (1996) PROZA96: an improved matrix correction program for electron probe microanalysis, based on a double Gaussian $\varphi(\rho z)$ approach. X-Ray Spectrom 27:3–10

Boudreau AE (1988) Investigations of the Stillwater Complex. IV. The role of volatiles in the petrogenesis of the J-M reef, Minneapolis Adit Section. Can Mineral 26:183–208

Boudreau AE (1999) Fluid fluxing of cumulates: the J-M reef and associated rocks of the Stillwater Complex, Montana. J Petrol 40:755–772

Boudreau AE (2016) The Stillwater Complex, Montana—overview and the significance of volatiles. Mineral Mag 80(4):585–637

Boudreau AE, McCallum IS (1985) Features of the picket pin Pt-Pd deposit. In: Czamanski J, Zientek M (eds) Stillwater Complex, Montana: geology and guide, vol 92. Montana Bureau of Mines and Geology, Special Pub., pp 346–357

Boudreau AE, McCallum IS (1986) Investigations of the Stillwater Complex, Part III. The picket pin Pt/Pd deposit. Econ Geol 81:1953–1975

Boudreau AE, McCallum IS (1989) Investigations of the Stillwater Complex: part V. Apatites as indicators of evolving fluid composition. Contrib Miner Petrol 102:138–153

Boudreau AE, McCallum IS (1992) Infiltration metasomatism in layered intrusions—an example from the Stillwater Complex, Montana. J Volcanol Geoth Res 52:171–183

Czamanske GK, Bohlen SR (1990) The Stillwater Complex and its anorthosites: an accident of magmatic underplating? Am Mineral 75:37–45

Czamanske GK, Scheidle DL (1985) Characteristics of banded-series anorthosites. In: Czamanski J, Zientek M (eds) Stillwater Complex, Montana: geology and guide, vol 92. Montana Bureau of Mines and Geology, Special Pub., pp 334–345

Czamanske GK, Zientek ML, Manning CE (1991) Low-K granophyres of the Stillwater Complex, Montana. Am Mineral 76:1646–1661

DePaolo DJ, Wasserburg GJ (1979) Sm-Nd age of the Stillwater Complex and the mantle evolution curve for neodymium. Geochim Cosmochim Acta 43:999–1008

Dick JM (2019) CHNOSZ: thermodynamic calculations and diagrams for geochemistry. Front Earth Sci 7:180. https://doi.org/10.3389/feart.2019.00180

Eales HV, Marsh JS, Mitchell AA, deKlerk WJ, Kruger FJ, Field M (1986) Some geochemical constraints upon models for the crystallization of the upper critical zone-main zone interval, northwestern Bushveld complex. Mineral Mag 50:567–582

Gitlin EC, Salpas PA, McCallum IS, Haskin LA (1985) Small scale compositional heterogeneities in Stillwater anorthosite II. Lunar and Planetary Science XVI. Lunar and Planetary Institute, Houston **(Extended abstract p. 272)**

Gualda GAR, Ghiorso MS (2015) MELTS_Excel: a microsoft excel-based MELTS interface for research and teaching of magma properties and evolution. Geochem Geophys Geosyst 16(1):315–324

Hayes B, Ashwal LD, Webb SJ, Bybee GM (2017) Large-scale magmatic layering in the Main Zone of the Bushveld Complex and Episodic Downward Magma Infiltration. Contrib Mineral Petrol 172(2–3):13. https://doi.org/10.1007/s00410-017-1334-4

Hess HH (1960) Stillwater igneous complex, Montana—a quantitative mineralogical study. Geological Society of America Memoir, 80. Geological Society of America, Boulder

Holland T, Blundy J (1994) Non-ideal interactions in calcic amphiboles and their bearing on amphibole-plagioclase thermometry. Contrib Miner Petrol 116:433–447

Irvine TN, Keith DW, Todd SG (1983) The J-M platinum-palladium reef of the Stillwater Complex, Montana: II. Origin by double-diffusive convective magma mixing and implications for the Bushveld Complex. Econ Geol Bull Soc Econ Geol 78:1287–1334

Johnson JW, Oelkers EH, Helgeson HC (1992) SUPCRT92: a software package for calculating the standard molal thermodynamic properties of minerals, gases, aqueous species, and reactions from 1 to 5000 bar and 0 to 1000. Comput Geosci 18:899–947. https://doi.org/10.1016/0098-3004(92)90029-Q

Latypov R (2019) Comment on "The Stillwater Complex: Integrating Zircon Geochronological and Geochemical Constraints on the Age, Emplacement History and Crystallization of a Large, Open-System Layered Intrusion" by Wall et al. (J. Petrology, 59, 153–190, 2018). J Petrol. https://doi.org/10.1093/petrology/egz014

Maaløe S (1987) Rhythmic layering of the Skaergaard intrusion. In: Parsons I (ed) Origins of igneous layering. NATO ASI Series (Series C: Mathematical and Physical Sciences), vol 196. Springer, Dordrecht

Maier WD (1995) Olivine okocrysts in Bushveld anorthosite: some implications for cumulate formation. Can Mineral 33:1011–1022

Maier WD, Karykowski BT, Yang S (2016) Formation of transgressive anorthosite seams in the Bushveld Complex via tectonically induced mobilisation of plagioclase-rich crystal mushes. Geosci Front 7(6):875–889

Mathez EA, Kinzler RJ (2017) Metasomatic chromite seams in the Bushveld and Rum layered intrusions. Elements 13:397–402

Mathison CI (1987) Pyroxene oikocrysts in troctolitic cumulates—evidence for supercooled crystallisation and postcumulus modification. Contrib Miner Petrol 97:228–236. https://doi.org/10.1007/BF00371242

McBirney AR (1987) Constitutional zone refining of layered mafic intrusions. In: Parsons I (ed) Origins of igneous layering. NATOASI Series (Series C: Mathematical and Physical Sciences), vol 186. Springer, Dordrecht, pp 437–452

McBirney AR, Sonnenthal EL (1990) Metasomatic replacement in the Skaergaard Intrusion, East Greenland: preliminary observations. Chem Geol 88:245–260

McCallum IS (1996) The Stillwater Complex. In: Cawthorn RG (ed) Layered intrusions. Elsevier Science B.V, pp 441–483

McCallum IS, Raedeke LD, Mathez EA (1980) Investigations in the Stillwater Complex: part I. Stratigraphy and structure of the Banded zone. Am J Sci 280A:59–87

Meurer WP, Klaber SA, Boudreau AE (1997) Discordant bodies from olivine-bearing zones III and IV of the Stillwater Complex, Montana—evidence for post-cumulus fluid migration in layered intrusions. Contrib Miner Petrol 130:81–92

Morse SA, Nolan KM (1984) Origin of strongly reversed rims on plagioclase in cumulates. Earth Planet Sci Lett 68:485–498

Mysen BO, Mibe K, Chou I-M, Bassett WA (2013) Structure and equilibria among silicate species in aqueous fluids in the upper mantle: experimental SiO_2–H_2O and MgO–SiO_2–H_2O data recorded in situ to 900 °C and 5.4 GPa. J Geophys Res Solid Earth 118:6076–6085. https://doi.org/10.1002/2013JB010537

Newton RC, Manning CE (2000) Quartz solubility in H_2O–NaCl and H_2O–CO_2 solutions at deep crust-upper mantle pressures and temperatures: 2–15 kbar and 500–900 °C. Geochim Cosmochim Acta 64(17):2993–3005

Newton RC, Manning CE (2016) Evidence for SiO_2–NaCl complexing in H_2O–NaCl solutions at high pressure and temperature. Geofluids 16:342–348

Nicholson DM, Mathez EA (1991) Petrogenesis of the Merensky Reef in the Rustenburg section of the Bushveld Complex. Contrib Miner Petrol 107:293–309

O'Driscoll B, Donaldson CH, Daly JS, Emeleus CH (2009) The roles of melt infiltration and cumulate assimilation in the formation of anorthosite and a Cr-spinel seam in the Rum Eastern Layered Intrusion. Lithos 111:6–20

Raedeke LD (1982) Petrogenesis of the Stillwater Complex. Ph.D. thesis. University of Washington, p 212

Raedeke LD, McCallum IS (1984) Investigations in the Stillwater Complex: part II. Petrology and petrogenesis of the ultramafic series. J Petrol 25(2):395–420

Salpas PA, Haskin LA, McCallum IS (1983) Stillwater anorthosites: a lunar analog? J Geophys Res 88(S01):B27–B39

Schmidt ME, Grunder AL, Rowe MC (2008) Segmentation of the cascade arc as indicated by Sr and Nd isotopic variation among diverse primitive basalts. Earth Planet Sci Lett 266:166–181

Sonnenthal EL (1992) Geochemistry of dendritic anorthosites and associated pegmatites in the Skaergaard Intrusion, East Greenland: evidence for metasomatism by a chlorine-rich fluid. J Volcanol Geotherm Res 52:209–230

Sverjensky DA, Harrison B, Azzolini D (2014) Water in the deep Earth: the dielectric constant and the solubilities of quartz and corundum to 60 kb and 1200 °C. Geochim Cosmochim Acta 129:125–145

Toplis MJ, Brown WL, Pupier E (1980) Plagioclase in the Skaergaard intrusion. Part 1: core and rim compositions in the layered series. Contrib Miner Petrol 155:329–340. https://doi.org/10.1007/s00410-007-0245-1

Wager LR, Brown GM, Wadsworth WJ (1960) Types of igneous cumulates. J Petrol 1:73–85

Wall CJ, Scoates JS, Weis D, Friedman RM, Amini M, Meurer WP (2018) The Stillwater Complex: integrating zircon geochronological and geochemical constraints on the age, emplacement history and crystallization of a large, open-system layered intrusion. J Petrol 59:153–190

Yoder HS, Tilley CE (1962) Origin of basalt magmas: an experimental study of natural and synthetic rock systems. J Petrol 3:342–532